Journal of Molecular Liquids 289 (2019) 111052

Contents lists available at ScienceDirect

Journal of Molecular Liquids

journal homepage: www.elsevier.com/locate/molliq

# Influence of $H_3O^+$ on the structure formation of oligomers in aluminium sols prepared from basic aluminium acetate: Experiments and computations

Chunlan Li, Wensheng Liu, Yunzhu Ma *

*National Key Laboratory of Science and Technology for National Defence on High-strength Structural Materials, Central South University, Changsha 410083, China*

ARTICLE INFO

*Article history:*
Received 16 February 2019
Received in revised form 5 May 2019
Accepted 26 May 2019
Available online 30 May 2019

*Keywords:*
FT-IR spectroscopy
$^{27}$Al NMR spectroscopy
Density functional theory
Oligomers
Aluminium sols
Basic aluminium acetate

ABSTRACT

In-depth insight into the structure of oligomers in sols plays an important role in determining the structure and properties of the final materials, such as aluminium borosilicate fibers, flakes, microspheres and composites. In this study, the influence of $H_3O^+$ on the structure formation of oligomers in sols prepared from basic aluminium acetate (BAA) was studied by Fourier-transform infrared spectroscopy (FT-IR), $^{27}$Al NMR spectroscopy and density functional theory (DFT) calculation. The results indicated that BAA consisting of tetrahedral Al species existed in dimeric form (BAA2-2). The polymerization of BAA2-2 was more thermodynamically favourable than its hydrolysis both in neutral and acidic solutions. The oligomers formed in neutral aqueous solution were beneficial to prepare different polymers with dendritic or three-dimensional structures. The oligomers formed in acidic solution ($H^+$/BAA = 0.5) were mostly linear tetramers composed of three octahedral and one tetrahedral Al species, which were beneficial to the spinnability of sols during the preparation of ceramic fibers. The addition of $H^+$ changed the electronic properties of Al(III) and significantly promoted the coordination ability of water and $Al^{3+}$, leading to an increase in the octahedral Al species and a great change in the structure of the sol. The DFT results were consistent with the experimental results, which provided a necessary theoretical guidance to improve the properties of aluminium sols and meet the needs of the final materials.



## 1. Introduction

Aluminium sols prepared from basic aluminium acetate can be used to produce alumina-based materials, such as aluminium borosilicate fibers, flakes, microspheres, and composites [1,2]. These alumina-based materials have been widely used as thermal insulation materials and the reinforcement of metals or ceramics for application in automotive, power engineering and aerospace industry [3,4], due to their excellent chemical and physical properties, especially their extreme lightweight and good flexible performance.

Sol-gel process has become one of the most attractive techniques for preparing alumina-based materials due to the inherent advantages of high purity, excellent homogeneity, low processing temperature and controllable chemical composition [5–7]. During the sol-gel progression, aluminium sol is the first essential elementary stage for preparing alumina-based materials and is also a crucial part of the whole process. For example, the structure of the oligomers in the sols during the sol-gel preparation of alumina-based fibers was found to be a key factor for the spinability of the sols [8–10]. Therefore, it is of great significance to characterize the structure of oligomers in aluminium sols at the molecular level.

The preparation of sol is based on the hydrolysis or condensation of precursors, and the structure of the oligomers in the sol depends on the kinetics of these chemical processes. Therefore, the hydrolysis and condensation reaction rates of the precursor are very important in the sol-gel process and can be influenced by many factors including the water amount, starting materials, pH, organic and inorganic additions, which have a great impact on the properties of the final materials [11,12]. In recent years, there have been many reports regarding the influence of pH on the hydrolysis and condensation reaction rates of precursors. Sakka et al. [13] reported that sols containing linear polymers could be obtained through the hydrolysis and condensation of Si $(OC_2H_5)_4$ when the amount water used was small and HCl was used as a catalyst, and these sols had good spinnability. However, sols containing non-linear or network colloidal polymers could be obtained through the hydrolysis and condensation of Si $(OC_2H_5)_4$ when $NH_4OH$ was used as catalyst, and these sols did not exhibit spinnability but prepared elastic bulk masses. Xintuo Chen and Lixia Gu [14] studied the dissolvability, homogeneity and spinnability of sols prepared from aluminium nitrate (AN), aluminium isopropoxide (AIP) and tetraethylorthosilicate (TEOS). These researchers found that with an increased amount of AN, AIP could only be dissolved under certain acidic conditions, and then, the hydrolysis

* Corresponding author.
*E-mail address:* zhuzipm@csu.edu.cn (Y. Ma).

https://doi.org/10.1016/j.molliq.2019.111052
0167-7322/

and condensation reactions occurred. The hydrolysis degree of AIP was related to the amount of AN. The preferable spinnable sols containing linear polymers could be prepared when the molar ratio of AIP/AN/TEOS was 9:3:4. Tan et al. [15] discussed the spinnability of alumina sols prepared with different amounts of aluminium powder and aluminium chloride. The pH of the sols changed with the $Al/AlCl_3 \cdot 6H_2O$ molar ratio. When the $Al/AlCl_3 \cdot 6H_2O$ molar ratio was 3.4 to 3.8 and the pH was in the range of 3.4–3.5, alumina sols containing the linear structure molecules optimal for spinning could be obtained. Based on these results, having the appropriate concentration of $H^+$ ions in the precursor solution is beneficial to the formation of linear structural polymers in sol. However, most of these analysis results are qualitative explanations based on experiment. Gaining in-depth insight into the mechanism of the $H^+$ ions still presents a great challenge, mainly because of the limited techniques for in situ characterization of sol. Quantum mechanical studies based on density functional theory (DFT) could be used to overcome this limitation and have been successfully applied to many studies on the structure, properties and reaction mechanisms of organic or inorganic compounds [16–19].

In our previous work [20], boron aluminium silicate fiber had been fabricated from basic aluminium acetate (BAA, $Al(OH)_2(OOCCH_3) \cdot 1/3H_3BO_3$ stabilized with boric acid), aluminium nitrate (AN), boric acid and silica sol by sol-gel method. In this process, AN acted not only as an aluminium salt, but also an acid. The release of $H^+$ ions during the hydrolysis of AN have a certain influence on the structure of aluminium sols. However, the influence mechanism of $H^+$ ions on the structure of the precursor sols prepared from BAA remains unclear. In this work, the colourless and transparent aluminium sols were prepared by sol-gel process using BAA as aluminium precursor and nitric acid as proton donor. The Fourier-transform infrared spectroscopy (FT-IR) and $^{27}Al$ NMR spectroscopy were used to characterize the components of aluminium sols prepared with different molar ratios of $HNO_3$ to BAA. To better understand the formation process of aluminium sols prepared from BAA at the molecular level and reveal the influence mechanism of $H^+$ ions on the structure of the precursor sols, DFT calculations were applied to study the hydrolysis and oligomerization of BAA under neutral and acidic conditions. In this sense, it is desirable to provide necessary theoretical guidance for controlling the experimental reaction conditions to further improve the properties of the aluminium precursor sols and meet the needs of the final materials. To the best of our knowledge, there are no detailed studies on the structure formation of oligomers in aluminium precursor sols prepared from BAA.

## 2. Experimental procedure

### 2.1. Preparation

The $HNO_3$ (65–68%) and deuterium oxide ($D_2O$, 99.9%) used were supplied by Aladdin; The dimethyl sulfoxide $d_6$ ($(CD_3)_2SO$, 99.96%) used was supplied by Sigma-Aldrich; The basic aluminium acetate (BAA, $Al(OH)_2(OOCCH_3) \cdot 1/3H_3BO_3$ stabilized with boric acid) was supplied by Strem Chemicals, Inc. The deionized water was prepared in the laboratory.

Variable amounts of $HNO_3$, with a molar ratio of $HNO_3/BAA = x$ ($x = 0$, 0.25, 0.5 and 0.75), were dissolved in deionized water and stirred for 10 min at 25 °C, and then, the BAA was added as the initial material to prepare the precursors. The mixed solution was stirred with a magnetic stirrer for 6 h to obtain the colourless and transparent aluminium sols for subsequent characterization.

### 2.2. Characterizations

The Fourier-transform infrared spectroscopy (FT-IR) was conducted at room temperature over the range of 400 to 4000 $cm^{-1}$ using a Nicolet 6700 Fourier-transform infrared spectrometer with the KBr pellet technique

The $^{27}Al$ NMR solution spectra were recorded at a frequency of 104.2 MHz on a Bruker Ascend-400 spectrometer. $[Al(H_2O)_6]^{3+}$ (1 M $Al(NO_3)_3$ solution) was used as the external reference (0 ppm).

### 2.3. Computational details

All the calculations reported in this study were carried out using the Gaussian 03 software package [21]. The geometry optimizations and vibrational frequency calculations of all the species involved in the hydrolysis and oligomerization of the precursor BAA were performed at the B3LYP functional and 6-311G** basis set level of DFT.

The solvent was water at 25 °C, and the effects were considered by the conductor-like polarizable continuum model (CPCM) [22–26] at the B3LYP/6-311G**. The CPCM method has been applied by Yu Takano and K. N. Houk [25] to the computations of the alkaline hydrolysis of methyl acetate in aqueous solution and the aqueous solvation free energies for a number of organic molecules. The results showed that the aqueous solvation effects agreed the best with the available experimental data. Cheng et al. [26] also successfully employed the CPCM method to consider the effects of bulk water, which made this method appropriate for studying the hydrolysis and polymerization of aluminium alkoxide. Intrinsic Reaction Coordinate (IRC) calculations [27,28] were performed to check the transition states (TS, one imaginary frequency) and confirm their connections between the right reactant (zero imaginary frequency) and product (zero imaginary frequency).

## 3. Results and discussion

### 3.1. Sol properties

The properties of precursor sols with different $HNO_3$ amount are listed in Table 1. The pH of the sol changed with the variety of $HNO_3$/BAA molar ratio. The addition of $HNO_3$ makes the aluminium sols transparent, and the reason may be that the presence of $HNO_3$ can promote the dissolution of BAA in aqueous solution.

### 3.2. FT-IR study of precursor sols

The structure of the BAA and the structure evolution of the aluminium sols prepared with different molar ratios of $HNO_3$/BAA (Table 1) were studied through a FT-IR analysis in the wavenumber range of 4000 to 400 $cm^{-1}$, and the results are illustrated in Fig. 1.

Persson et al. [29] comprehensively characterized Al(III)-acetate complexation with the composition $[Al_2(OH)_2OAc]^{3+}$ by attenuated total reflectance FT-IR spectroscopy. The analysis of the asymmetric (1581 $cm^{-1}$) and symmetric $\nu_{C-O}$ bands (1474 $cm^{-1}$) originating from the coordinated acetate ions suggested the existence of a complex in which the acetate ion acts as a bridging ligand in a *syn-syn* geometry.

**Table 1**
Properties of precursor sols with different $HNO_3$ amount.

| Sample | $H_2O$ (g) | $D_2O$ (g) | $HNO_3$/BAA (molar ratio) | pH of sols | Appearance of sols |
|---|---|---|---|---|---|
| Sol 1 (Sol 5) | 8.0 (7.2) | 0 (0.8) | 0 | 4.96 | Opaque |
| Sol 2 (Sol 6) | 8.0 (7.2) | 0 (0.8) | 0.25 | 3.96 | Transparent |
| Sol 3 (Sol 7) | 8.0 (7.2) | 0 (0.8) | 0.5 | 3.41 | Transparent |
| Sol 4 (Sol 8) | 8.0 (7.2) | 0 (0.8) | 0.75 | 2.98 | Transparent |

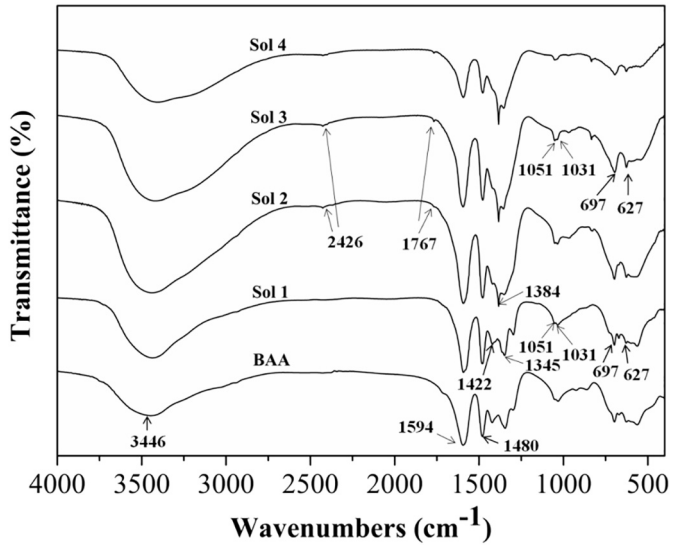


**Fig. 1.** FT-IR spectra of BAA and aluminium sols with different molar ratios of $HNO_3$/BAA, Sol 1, 0; Sol 2, 0.25; Sol 3, 0.5; Sol 4, 0.75.

According to Persson's studies, and subtracting the standard infrared spectrum of BAA, the BAA materials contain acetate ions that act as bridging ligands, forming the strong bands at 1594 $cm^{-1}$ and 1480 $cm^{-1}$ ($\Delta = 114\ cm^{-1}$) shown in Fig. 1.

For the sol samples, the band at 3446 $cm^{-1}$ attributed to O—H stretch [30]. The band at 1384 $cm^{-1}$ ascribed to distorted $NO_3^-$ stretch vibrations is observed in Sol 2 [10,31]. This band increases in intensity with increasing amounts of $HNO_3$, which leads to decreasing intensities for the bands at 1422 $cm^{-1}$ and 1345 $cm^{-1}$ corresponding to B—O bond asymmetric stretching of $BO_3$ units and C—H bond deformation of $CH_3$ units [32–35]. The band at 1031 $cm^{-1}$ is assigned to the Al-OH deformation mode [35]. The band at 1051 $cm^{-1}$ corresponds to Al—O—C stretching vibrations [36]. Relative to the intensity of the band at 1051 $cm^{-1}$, the band at 1031 $cm^{-1}$ tends to decrease slightly in intensity with increasing amounts of $HNO_3$, which may be due to protonation of Al-OH by $H^+$ ions ionized from $HNO_3$. In addition, the intensities of the bands at 697 $cm^{-1}$ and 627 $cm^{-1}$ from the Al—O stretch in AlO6 increase proportionally from Sol 1 to Sol 3 [37]. Two small peaks at 2426 $cm^{-1}$ and 1767 $cm^{-1}$ attributed to free carboxylic acid vibrations [10,29] can be found in Sol 2, Sol 3 and Sol 4, indicating that a few BAA might start to hydrolyse when the molar ratio of $HNO_3$ to BAA is 0.25. The intensities of all the bands for Sol 4 relatively decrease, which may be due to the excessive concentration of $NO_3^-$.

As mentioned above, BAA containing an acetate ion acts as a bridging ligand might in dimeric form. With increasing molar ratio of $HNO_3$/BAA, the amount of the octahedral Al species increases, and the BAA molecules tend to hydrolyse slightly in aqueous solution.

### 3.3. $^{27}$Al NMR study of precursor sols

The structure of BAA was analysed by $^{27}$Al NMR spectroscopy, and the samples of Sol 5, Sol 6, Sol 7 and Sol 8 (Table 1) were also analysed to study the local structure of Al in the precursor sols, shown in Fig. 2.

The $^{27}$Al NMR spectra of the BAA samples show that the BAA exists in tetrahedral form (Fig. 2A, curve 1, ~70 ppm resonance relative to Al $(NO_3)_3$). However, a broad peak (~65 ppm) and a broad shoulder peak (~9 ppm) observed in the spectra of BAA prepared with $D_2O$ (Fig. 2A, curve 2). The two broad peaks are attributable to the tetrahedral and octahedral Al species [37,38], respectively. Obviously, the solvent had a certain influence on the Al-speciation in BAA.

For the sol samples (Fig. 2B), there are two broad peaks (~5 ppm and ~65 ppm, attributed to the octahedral and tetrahedral Al species, respectively) in Sol 1. With increasing amounts of $HNO_3$, the $Al^{3+}$ oligomer (resonance at ~5 ppm) content increases; the content of tetrahedral Al species (resonance at ~65 ppm) decreases in contrast. When the molar ratio of $HNO_3$ to BAA is 0.25 (Sol 2), small, sharp signals at ~0.86 ppm due to $Al^{3+}$ monomers or dimers can be seen, and the relative content of the octahedral Al species increases above that of the tetrahedral Al species. However, when the molar ratio of $HNO_3$ to BAA is 0.75 (Sol 4), the relative content of $Al^{3+}$ monomers or dimers (resonance at 0.86 ppm) is much higher than that of oligomers (resonance at ~5 ppm), and the content of tetrahedral Al species (resonance at ~65 ppm) is almost zero, implying that the relative content of $Al^{3+}$ oligomers (resonance at ~5 ppm) reaches the maximum when the molar ratio of $HNO_3$ to BAA is 0.5.

Monomer and oligomer have different degrees of polymerization; the existence and relative amounts of these species play a crucial role in the structure and properties of the sol [9]. In these sol samples, the relative content of $Al^{3+}$ oligomers in Sol 3 is the highest, while the $Al^{3+}$ of oligomer in Sol 4 is decreased instead. The addition of $HNO_3$ has a great influence on the Al-Speciation in precursor sols.

### 3.4. Molecular geometry

From the FT-IR analysis results, the BAA existed in dimeric form. The molecular structures of all the possible dimers (isomers) for BAA in aqueous solution were listed and optimized (Fig. 3A), and a vibrational frequency analysis at the same level of theory was performed; the lowest frequencies and Gibbs free energies of isomers for BAA are listed in Table 2. According to Table 2, no imaginary vibrational frequencies are

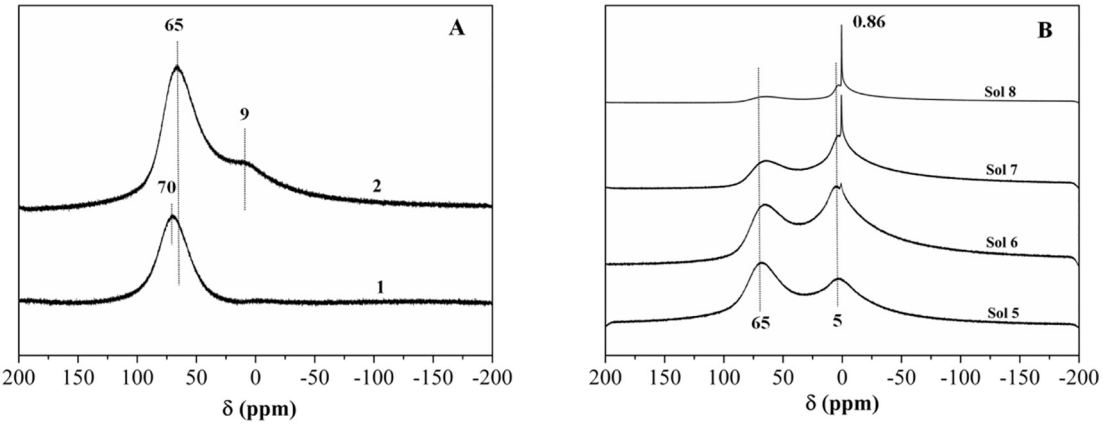


**Fig. 2.** (A) $^{27}$Al NMR spectra of BAA prepared by $(CD_3)_2SO$ (spectra 1) and $D_2O$ (spectra 2); (B) $^{27}$Al NMR spectra of different aluminium sols with different molar ratios of $HNO_3$/BAA prepared by $H_2O + D_2O$, Sol 5, 0; Sol 6, 0.25; Sol 7, 0.5; Sol 8, 0.75.

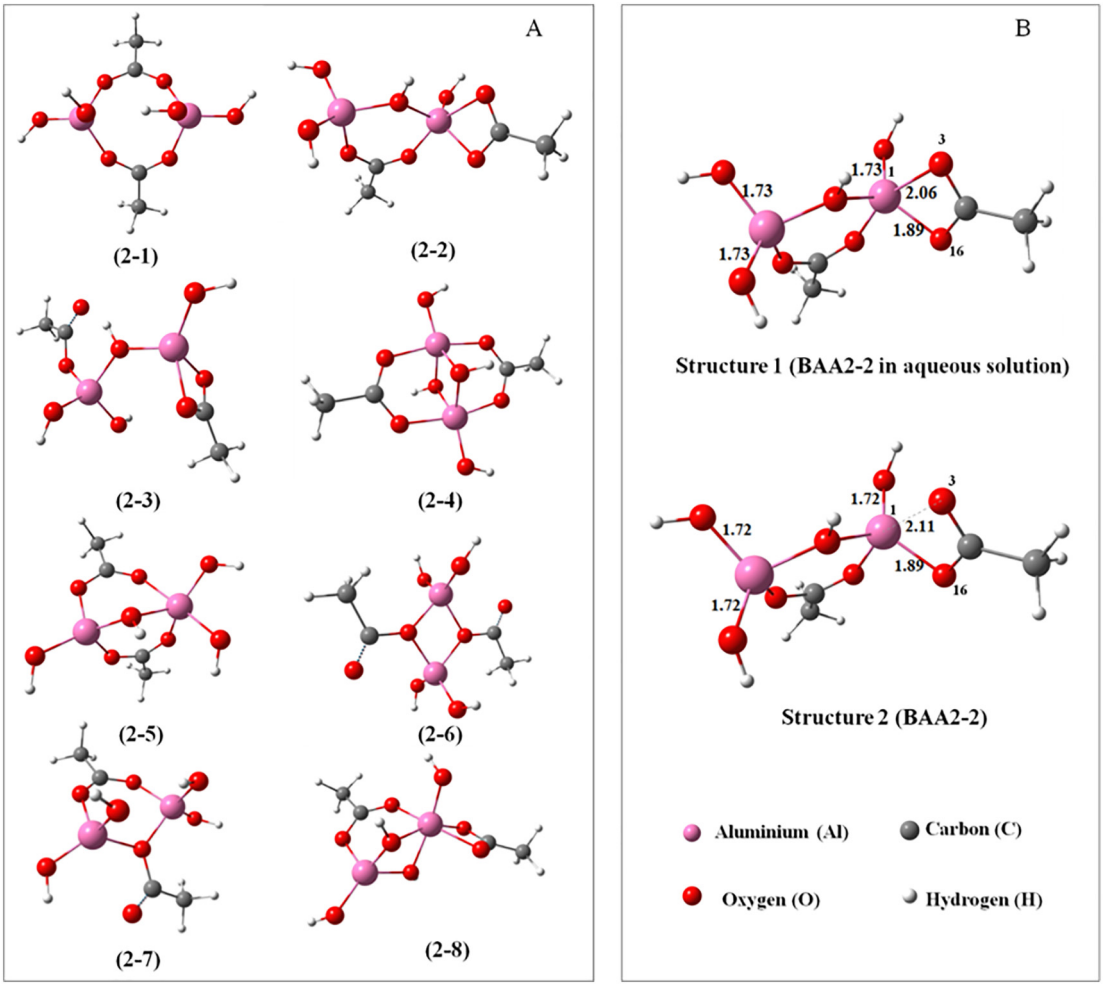


**Fig. 3.** (A) Optimized geometries of isomers for BAA in aqueous solution; (B) optimized geometries and selected bond distances of BAA2-2 with and without aqueous solutions. The selected bond lengths are in Å, this unit is uniformly employed in all figures. Note: aluminium in pink, carbon in dark grey, oxygen in red, and hydrogen in light grey.

observed for any species, and the Gibbs free energies of 2-2 (Fig. 3A, 2-2, named BAA2-2) and 2-8 (Fig. 3A, 2-8, named BAA2-8) are relatively low. BAA2-2 is more stable than BAA2-8 by 18.5 kJ/mol. This large energy difference indicates that BAA2-2 comprised the majority in the aqueous solution. The BAA2-2 contained bridging acetate bidentate, and the calculated bands at 1595 $cm^{-1}$ and 1493 $cm^{-1}$ are attributed to the asymmetric and symmetric stretching vibrations of bridging bidentate $COO^{-1}$, respectively (Fig. 4). This is in accord with the 1998-year study of P. Persson, M. Karlsson, and L.O. Öhman about coordination of acetate to Al(III) in aqueous solution and at the water-aluminum hydroxide interface [29]. It was done by a potentiometric and attenuated total reflectance FT-IR study. But experimental study [29] considered a bit different system and modeling. The present infrared results obtained by the DFT calculation support the stretching modes of bridging bidentate $COO^{-1}$. As shown in Fig. 4, both the infrared bands of bridging bidentate $COO^{-1}$ obtained by experiment and DFT calculation are the most prominent in the FT-IR spectrum and serve as a key assignment for the BAA. However, the band peaks of other characteristic groups are slightly different from the experiments. A possible explanation is that the samples might be affected by the water molecules and the interactions between the sample molecules. For example, there is no hydrogen bonding in BAA2-2 molecule itself, and the stretching vibration of O—H (Al—OH) appears at 3822 $cm^{-1}$. In experiments, however, BAA2-2 molecules can form hydrogen bonds with water molecules, resulting in the stretching vibration of O—H (Al—OH) at 3446 $cm^{-1}$. In addition, BAA2-2 molecule is independent in DFT calculation, which is mainly composed of AlO4 species (866 $cm^{-1}$ and 775 $cm^{-1}$). The peaks at 1057 $cm^{-1}$, 727 $cm^{-1}$ and 682 $cm^{-1}$ are corresponded to the deformation vibrations of O—H (Al—OH). In the experiment, the deformation vibrations of O—H (Al—OH) and Al—O (AlO4) in BAA2-2 may overlap with that of $BO_3$ and $NO_3$ (400 $cm^{-1}$–1000 $cm^{-1}$). The vibrational frequencies calculated by DFT are generally higher than the FT-IR experimental results due to the systematic error, which can be avoided by scaling the calculated frequencies according to the empirical factor, and thus the scaled calculated frequencies are much closer to the experimental results [39,40]. In this work, the calculated vibrational frequencies of the main characteristic groups in BAA (including the main characteristic groups of oligomers obtained by BAA) are in good agreement with the FT-IR experimental results, which can be used without scaling.

**Table 2**
Lowest frequency and gibbs free energy of baa isomers.

| Species | Frequency/$cm^{-1}$ | Gibbs free energy/hartree |
|---|---|---|
| 2–1 | 43 | −1245.766387 |
| 2–2 | 20 | −1245.778253 |
| 2–3 | 30 | −1245.748899 |
| 2–4 | 37 | −1245.765699 |
| 2–5 | 33 | −1245.764312 |
| 2–6 | 25 | −1245.739667 |
| 2–7 | 45 | −1245.750570 |
| 2–8 | 35 | −1245.771197 |

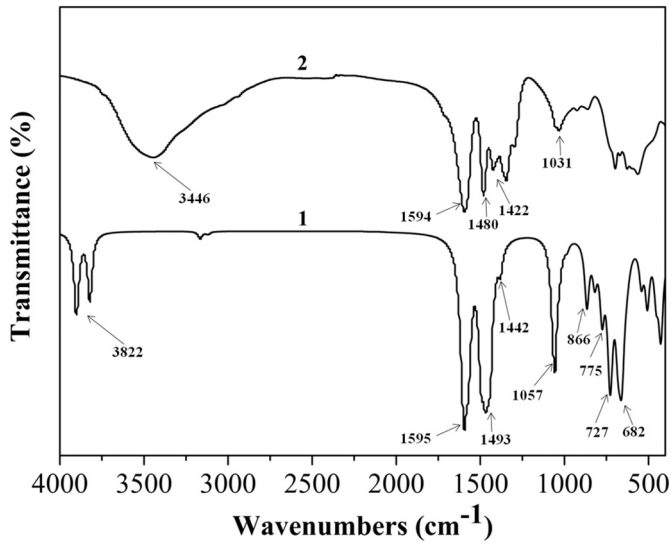


**Fig. 4.** IR spectra of BAA2-2 (1) provided by DFT calculation; (2) provided by experiment.

Fig. 3B shows the optimized geometries and selected bond distances of BAA2-2 with and without aqueous solution. BAA2-2 consists of four-coordinate aluminium (Fig. 3B, structure 2), which is consistent with the $^{27}$Al NMR study. The bond length between Al1 and O3 is shorted from 2.11 to 2.06 Å due to solvent effects. However, the bond length between Al1 and O3 in structure 1 is still far longer than the sum radius of $Al^{3+}$ and $O^{2-}$. The bond energy of Al1—O3 is very weak, suggesting that the breaking or formation of Al1—O3 bonds has only a small effect on the electron density (surface energetics and surface properties) of $Al1^{3+}$ in BAA2-2. The BAA2-2 in aqueous solution is also mainly the tetrahedral Al-speciation.

### *3.5. Structure formation of precursor sols when the ratio of $H^+$ to BAA2-2 is 0 in aqueous solution ($H^+$/BAA = 0, pH = 4.96)*

#### *3.5.1. Coordination of water to BAA2-2*

$Al^{3+}$ easily coordinates with water molecules to form tetrahedral or octahedral Al species. Therefore, the stabilities of several BAA2-2·$(H_2O)_n$·(n = 1–3) adducts were investigated. Fig. 5 depicts the geometrical parameters and free energy differences of BAA2-2·$(H_2O)_n$ (n = 1–3) in aqueous solution. Fig. 5 shows that BAA2-2·$H_2O$ is more stable than its isomer BAA2-2·$(H_2O)_{1\text{-}1}$ by 9.3 kJ/mol, implying that the O3 atom on acetate is more likely to form hydrogen bond with the coordinated water molecule. The coordination of water molecule has a certain effect on the binding mode of acetate in BAA2-2. However, the gradual addition of one and two $H_2O$ molecules to BAA2-2 yields stabilization energies of only 8.3 and 3.3 kJ/mol, respectively, indicating that there might be a few BAA2-2 coordinating with water molecules to form BAA2-2·$(H_2O)_2$ in neutral aqueous solution.

#### *3.5.2. Hydrolysis of the BAA2-2*

The hydrolysis of the precursor BAA2-2 was investigated in this work. The optimized geometrical parameters and the PES profile involved in the hydrolysis of BAA2-2 in neutral aqueous solution are described in Fig. 6. One water molecule is coordinated to the Al1 atom of BAA2-2, which is fully optimized to form $H_2O$-IM1, where the distance of Al1—O25 is 2.00 Å and the hydrogen bond (O25—H26—O3) is formed. Compared with BAA2-2 + $H_2O$, the Gibbs free energy decreases 8.3 kJ/mol. Then, H26 shifts from O25 to O16 via $H_2O$-TS1 to form $H_2O$-IM2, with an estimated energy barrier of 91.7 kJ/mol. Fig. 6 shows that the free energies of the products are higher than those of BAA2-2 + $H_2O$, which is energetically unfavourable. Therefore, the formation of hydrogen bond (O25—H26—O3) makes it difficult for H26 to transfer to O16, and the hydrolysis of precursor BAA2-2 is very difficult.

#### *3.5.3. Oligomerization of the BAA2-2*

Since the BAA2-2 molecule has three active hydroxyl groups, which all have the opportunity to combine with $Al^{3+}$ of other BAA2-2 molecules to form new oligomers, there are several reaction routes for the polymerization of BAA2-2. The optimized geometrical parameters and the PES profile involved in the polymerization of BAA2-2 in neutral aqueous solution are listed in Fig. 7.

From Fig. 7, it can be seen that the potential barrier of the first, the second and the third route is 113.2 kJ/mol, 55.4 kJ/mol and 45.0 kJ/mol, respectively. The third route seems to be more energetically favourable than other two routes. However, the free energy of IM1-1 is much lower than that of IM1-3, suggesting that IM1-1 will be generated first for the polymerization of BAA2-2. IM1-1 is the most stable species

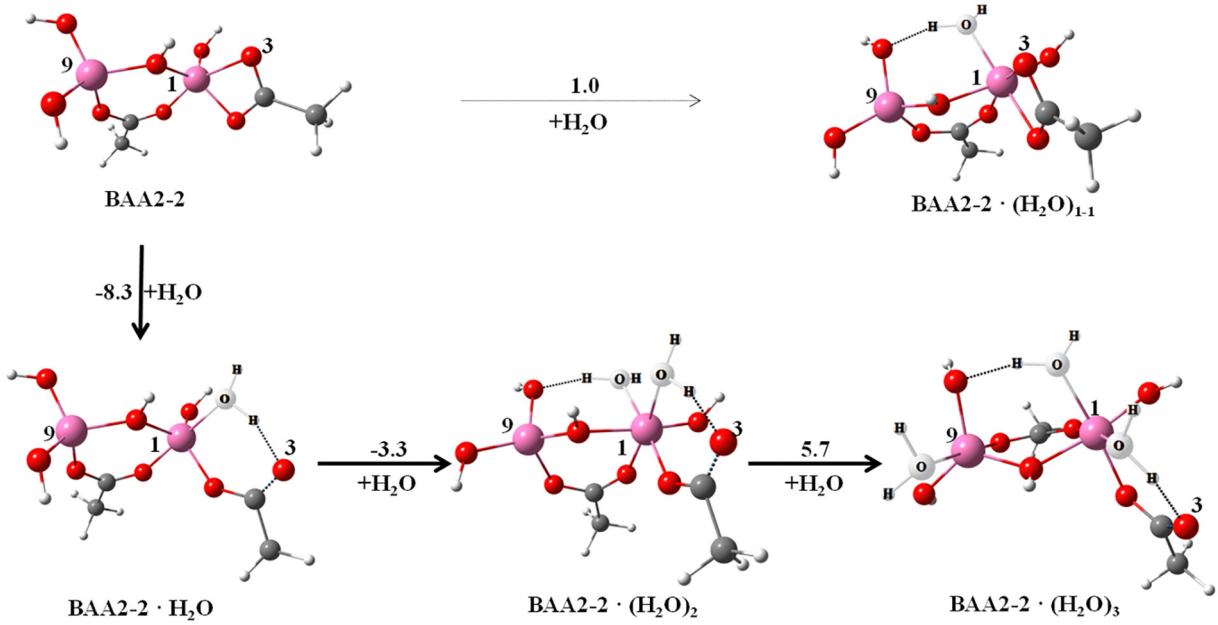


**Fig. 5.** Geometrical parameters and free energy differences of BAA2-2·$(H_2O)_n$ (n = 1–3) in neutral aqueous solution. The relative energies are in kJ/mol, this unit is uniformly employed in all figures.

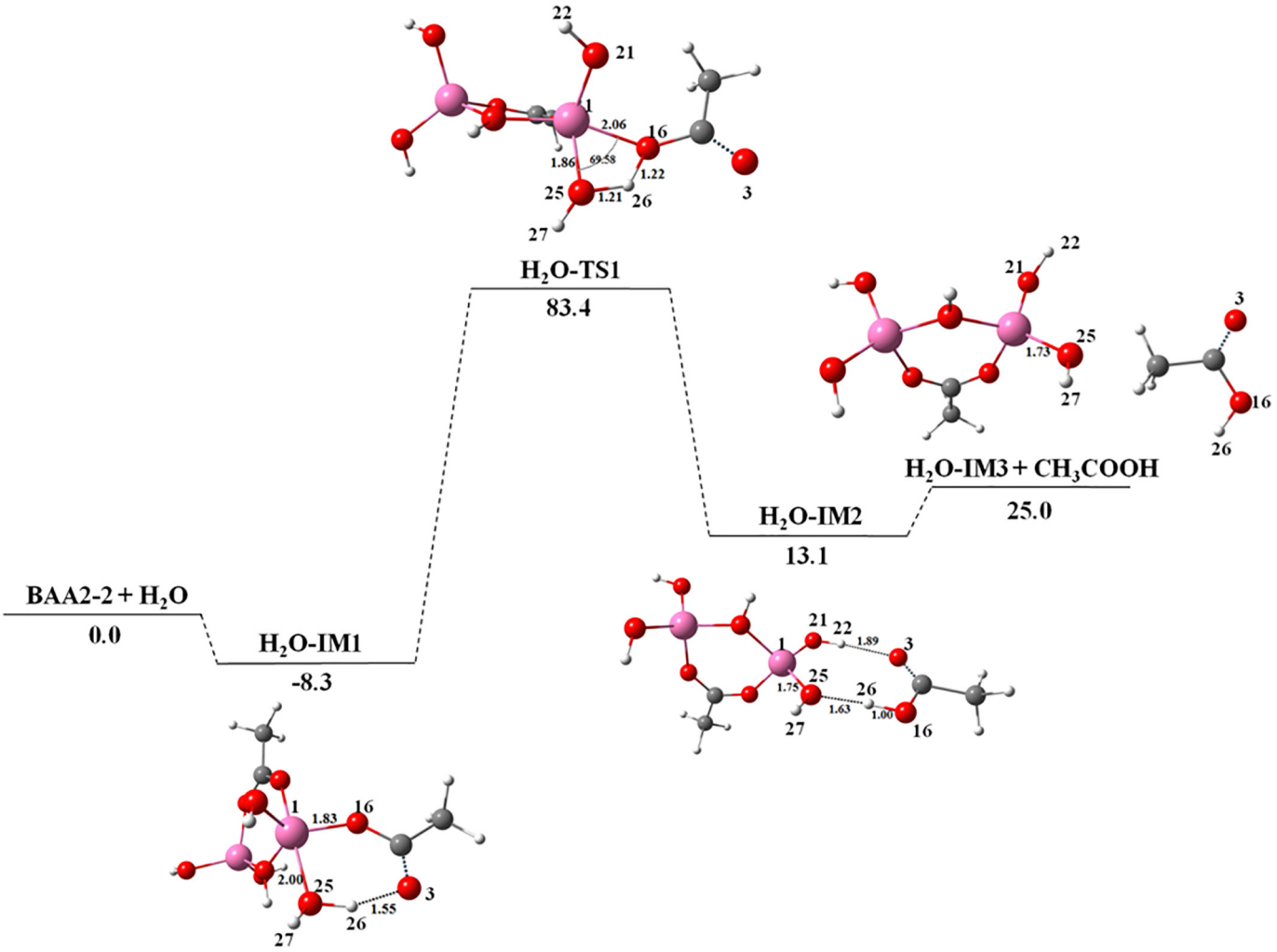


**Fig. 6.** Optimized geometrical parameters and the PES profile involved in the hydrolysis of BAA2-2 in neutral aqueous solution.

in this route since the free energy of the products IM3-1 + $H_2O$ is much higher than that of BAA2-2 + BAA2-2. In addition, Two BAA2-2 molecules can also bind together to form the isomer i-IM1-1, which is stable than IM1-1 just by 1.0 kJ/mol. This small energy difference shows that both IM1-1 and i-IM1-1 can be obtained in this process. The lowest frequencies and Gibbs free energies of IM1-1 and i-IM1-1 are presented in Table 3. The assignment of frequencies in the IR spectra of IM1-1 and i-IM1-1 are listed in Table 4. The bands at 1048 $cm^{-1}$, 999 $cm^{-1}$ are assigned to the O—H (Al—OH) deformation mode. The bands at 3465 $cm^{-1}$, 3501 $cm^{-1}$ are attributed to O—H (Al—OH) stretching mode, where the hydroxyl group forms a hydrogen bonding with the adjacent oxygen atom. These calculation results are agreed with the FT-IR experimental results.

These computation results indicate that, when the $H^+$/BAA molar ratio is 0, BAA2-2 is difficult to hydrolyse in aqueous solution. The BAA2-2 molecules are spontaneously polymerized to form polyhydroxyl oligomers. These polyhydroxyl oligomers can further react with themselves or BAA2-2 molecules to form different polymers with dendritic or other three-dimensional structures.

### *3.6. Structure formation of precursor sols when the ratio of $H^+$ to BAA2–2 is 1 in aqueous solution ($H^+$/BAA = 0.5, pH = 3.41)*

In this study, nitric acid was used as the proton donor in the synthesis of the precursor sols. In the initial stage, $H^+$ protonates a hydroxyl group of BAA2-2 to form intermediate BAA2-2-H, as shown in Fig. 8. Among the three optimized configurations of BAA2-2-H, BAA2-2-H (b) is more stable than BAA2-2-H (a) by 2.2 kJ/mol, and BAA2-2-H (c) is more stable than BAA2-2 (b) by 7.4 kJ/mol. These energy differences indicate that BAA2-2-H (c) is a more preferable configuration than BAA2-2-H (a) and BAA2-2-H (b).

#### *3.6.1. Coordination of water to BAA2-2-H*

Fig. 9 illustrates the geometrical parameters and free energy difference of BAA2-2-H·$(H_2O)_n$ (n = 1–3) in aqueous solution. Fig. 9 shows gradually adding one and two $H_2O$ molecules to BAA2-2-H stabilizes the Al complex by 59.7 and 25.1 kJ/mol, respectively. BAA2-2-H·$(H_2O)_2$ is more stable than the isomer BAA2-2-H·$(H_2O)_{2\text{-}1}$ by 18.7 kJ/mol. The coordination of the second water molecule makes the O16 atom in BAA2-2-H·$(H_2O)_2$ disconnecting from the Al1 atom and forms hydrogen bond with a water molecule. BAA2-2-H·$(H_2O)_2$ is the most stable hydrate in acidic aqueous solution. Clearly, the existence of $H^+$ changes the electronic properties of Al(III) and significantly promotes the coordination ability of water to $Al^{3+}$. Therefore, BAA2-2-H·$(H_2O)_2$ is the most stable species in aqueous solution.

#### *3.6.2. Hydrolysis of the BAA2-2-H*

As shown in Fig. 8, from BAA2-2 to BAA2-2-H(c), the bond length between Al1 and O3 is shortened from 2.06 to 1.95 Å, indicating that the stability of Al1—O3 in BAA2-2 increased due to the presence of $H^+$. Therefore, BAA2-2-H is more difficult to hydrolyse by one water molecule than BAA2-2. However, we can add two water molecules to the

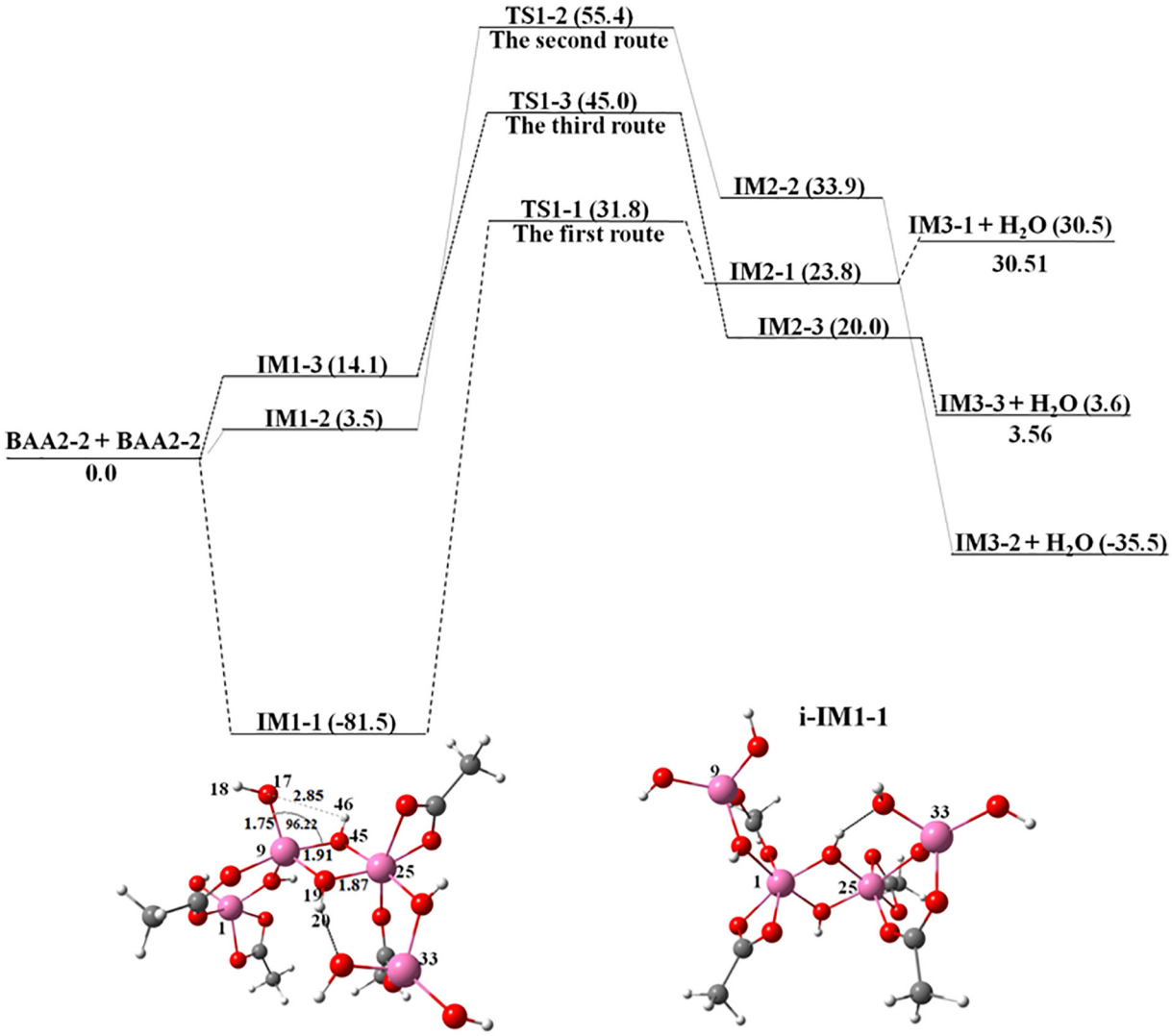


**Fig. 7.** Optimized geometrical parameters and the PES profile involved in the polymerization of BAA2-2 in neutral aqueous solution.

**Table 3**
Lowest frequency and Gibbs free energy of IM1-1 and i-IM1-1.

| Species | Frequency/cm$^{-1}$ | Gibbs free energy/hartree |
|---|---|---|
| IM1-1 | 12 | −2491.587517 |
| i-IM1-1 | 13 | −2491.587882 |

central Al1 atoms of BAA2-2-H to study the hydrolysis kinetics of BAA2-2-H. The optimized geometric parameters and the PES profile of this channel are shown in Fig. 10.

Fig. 10 shows two water molecules are coordinated to the Al1 atom to form H-2$H_2O$-IM1, where the bond lengths of Al1—O26 and

**Table 4**
Unscaled calculations for vibrational frequencies, IR intensities and band assignments of IM1-1 and i-IM1-1.

| Species | Assignment | Vibrational frequency (experimental frequency)/cm$^{-1}$ | IR intensity/km·mol$^{-1}$ |
|---|---|---|---|
| IM1-1 | $CH_3$ (def.) | 1442 (1422) | 276 |
| | OCO (asym., str.) | 1603 (1593) | 1148 |
| | OCO (sym., str.) | 1492 (1480) | 347 |
| | OH (Al-OH, def.) | 1048 (1031) | 450 |
| | OH (Al-OH, str.) | 3465 (3436) | 1106 |
| | Al-O (AlO6, str.) | 637 (627) | 201 |
| | | 688 (697) | 388 |
| i-IM1-1 | $CH_3$ (def.) | 1441 (1422) | 320 |
| | OCO (asym., str.) | 1603 (1593) | 943 |
| | OCO (sym., str.) | 1487 (1480) | 353 |
| | OH (Al-OH, def.) | 999 (1031) | 293 |
| | OH (Al-OH, str.) | 3501 (3436) | 1070 |
| | Al-O (AlO6, str.) | 639 (627) | 233 |
| | | 699 (697) | 307 |

def., deformation mode; str., stretching mode; asym., asymmetric; sym., symmetric.

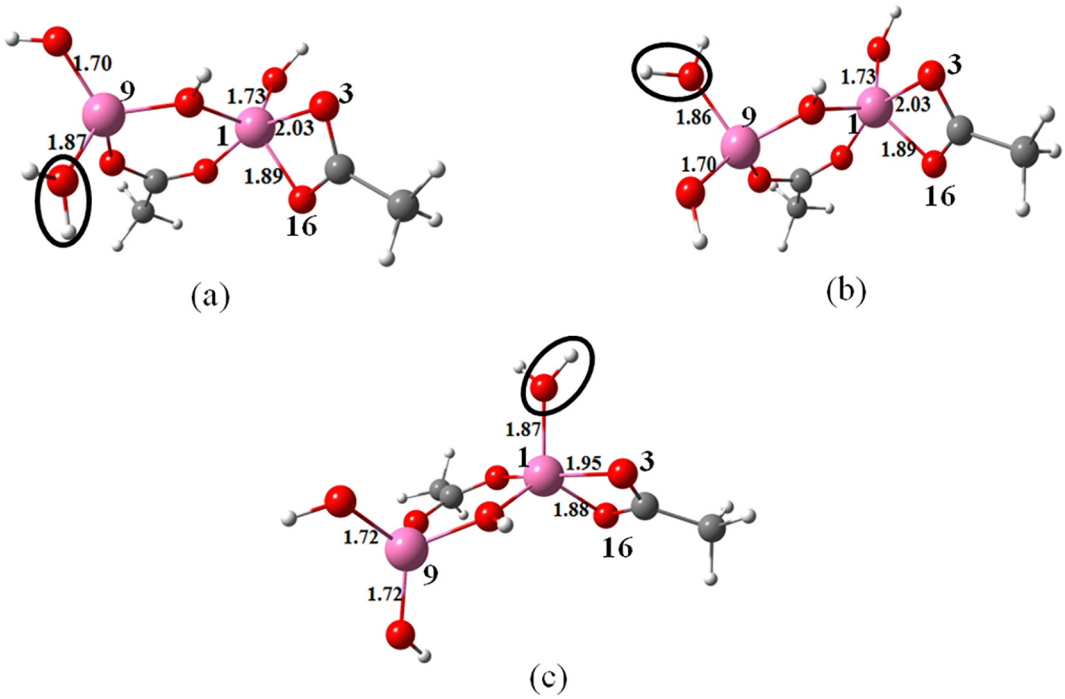


**Fig. 8.** Optimized geometries and selected bond distances of BAA2-2-H in aqueous solution.

Al1—O29 are 1.94 and 1.99 Å, respectively. Meanwhile, the O16 atom breaks off from the Al1 atom and forms a hydrogen bond with another water molecule. Then, the H31 atom shifts from O29 to O3 via H-2$H_2O$-TS1, leading to the formation of H-2$H_2O$-IM2. Subsequently, the $CH_3COOH$ molecule leaves H-2$H_2O$-IM2 via a barrierless process, generating H-2$H_2O$-IM3 and $CH_3COOH$. The PES shows that the energy barrier of this process is 102.3 kJ/mol. However, the high exothermicity of the formation of H-2$H_2O$-IM1 may completely compensate for this barrier; thus, this process may be energetically favourable, indicating that two water molecules make the hydrolysis of BAA2-2-H possible.

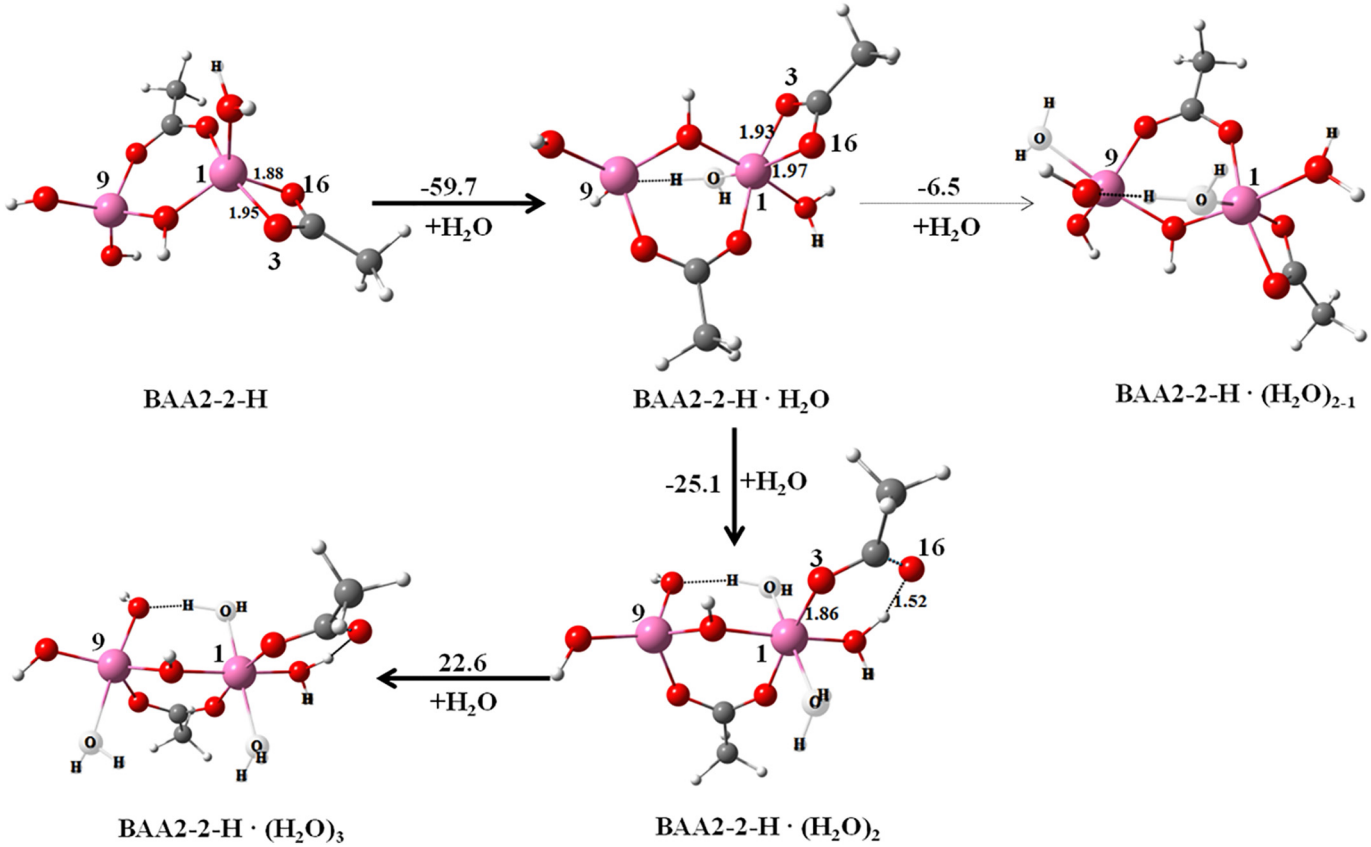


**Fig. 9.** Geometrical parameters and free energy difference of BAA2-2-H·$(H_2O)_n$ (n = 1–3) in aqueous solution.

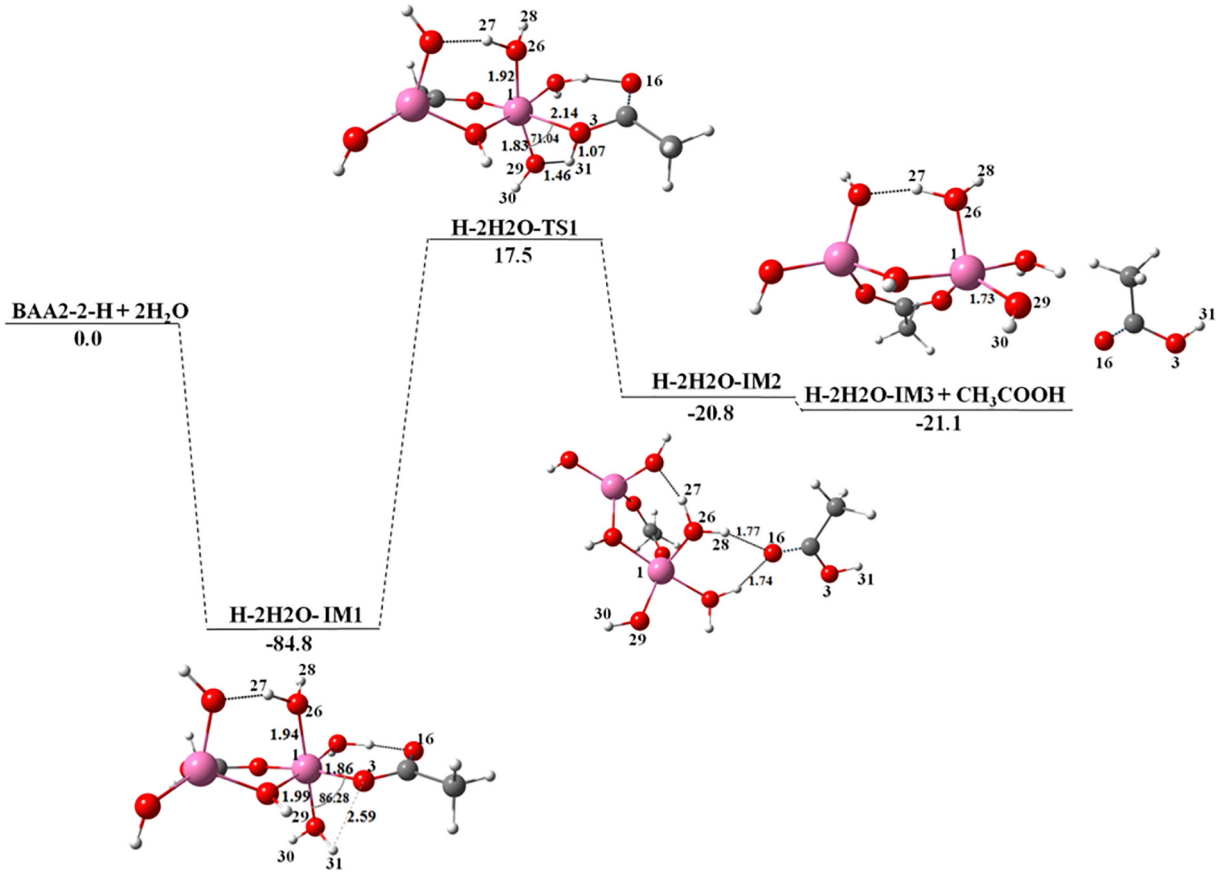


**Fig. 10.** Optimized geometrical parameters and the PES profile involved in the hydrolysis of BAA2-2-H in aqueous solution.

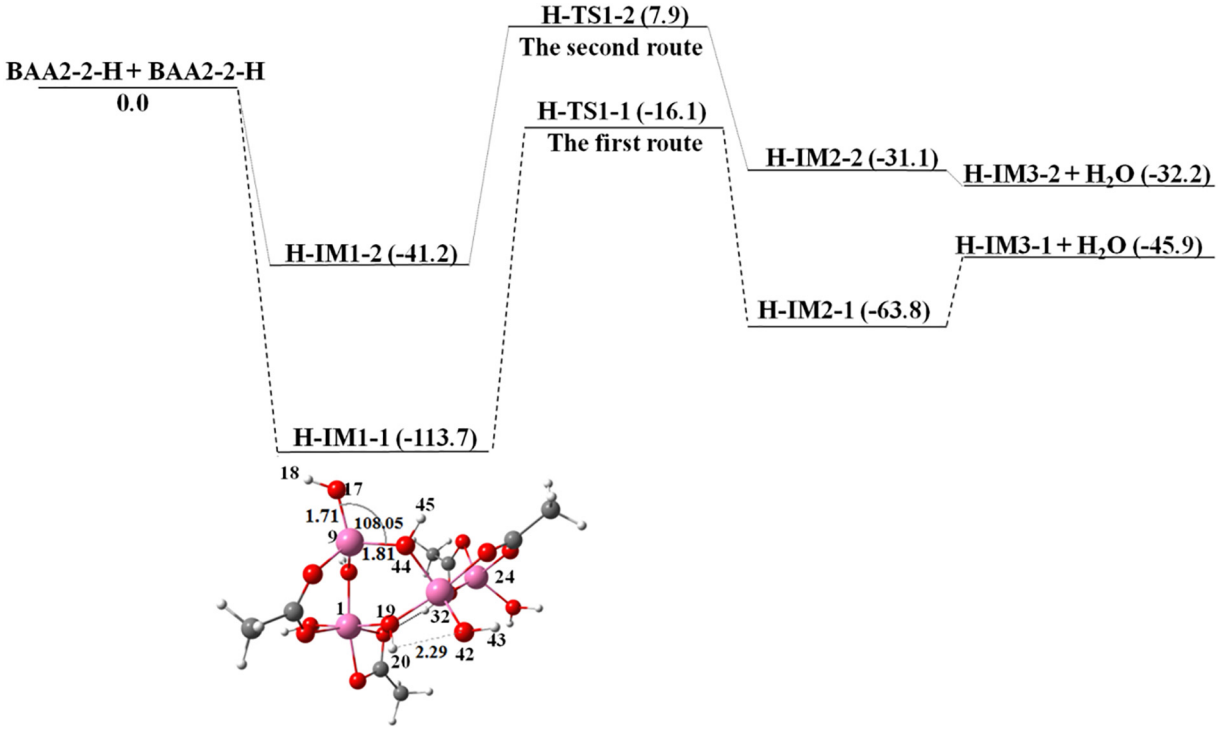


**Fig. 11.** Optimized geometrical parameters and the PES profile involved in the polymerization of BAA2-2-H in aqueous solution.

*3.6.3. Oligomerization of the BAA2-2-H*

The optimized geometrical parameters and the PES profile involved in the polymerization of BAA2-2-H in aqueous solution are depicted in Fig. 11. Fig. 11 shows that there are two reaction routes for the polymerization of BAA2-2-H, and the second route is more energetically favourable than the first route, because the barrier of this route is 49.1 kJ/mol, much lower than that of the first route (97.6 kJ/mol). However, for the first reaction route, the free energy of H-IM1-1 is much lower than that of H-IM1-2, indicating that H-IM1-1 will be generated first for the polymerization of BAA2-2-H. In forming intermediate H-IM1-1, the tetra-coordinated Al atoms of BAA2-2-H are linked together by a bridging O44 atom, and this procedure decreases the free energy by 113.7 kJ/mol. Evidently H-IM1-1 has the lowest energy, which is the most stable species in this route.

Since the Al9, Al24 and Al32 atoms in H-IM1-1 are five-coordinate and four-coordinate, the stabilities of several H-IM1-1·$(H_2O)_n$·(n = 1–4) adducts were investigated. Fig. 12 shows the geometrical parameters and free energy differences of H-IM1-1·$(H_2O)_n$ (n = 1–4) in aqueous solution. Compared with H-IM1-1, the energy differences of H-IM1-1·$(H_2O)_n$ (n = 1–4) decrease by 37.8 kJ/mol, 64.8 kJ/mol, 83.2 kJ/mol, and 117.5 kJ/mol, respectively. The H-IM1-1·$(H_2O)_4$ species comprise the majority in acidic aqueous solution. Gradually adding the third and the fourth water molecules to H-IM1-1 cause the O28 atom in H-IM1-1·$(H_2O)_3$ and O16 atom in H-IM1-1·$(H_2O)_4$ disconnecting from the Al24 and Al1 atoms to form hydrogen bonds, respectively. Table 5 demonstrates the assignment of frequencies in the IR spectra of H-IM1-1·$(H_2O)_4$. The band at 1030 $cm^{-1}$ is assigned to the O—H (Al—OH) deformation mode. Due to the formation of hydrogen bonding, the O—H stretching vibration of water molecule occurs at 3401 $cm^{-1}$. Compared with oligomers formed under neutral condition, the IR intensity of O—H (Al—OH) in H-IM1-1·$(H_2O)_4$ is relatively decreased, while that of Al—O (AlO6) is relatively increased. These DFT calculations are consistent with the FT-IR experimental results.

From our computation, BAA2-2-H may be hydrolysed in aqueous solution. The existence of $H^+$ changes the electronic properties of Al(III) and significantly promotes the coordination ability of water to $Al^{3+}$. BAA2-2-H·$(H_2O)_2$ is more stable than BAA2-2-H in aqueous solution. However, the formation of H-IM1 is more thermodynamically favourable than that of BAA2-2-H·$(H_2O)_2$ in aqueous solution. When the ratio of $H^+$/BAA2-2 is 1 ($H^+$/BAA is 0.5), the coordination of water molecules with $Al^{3+}$ prevent the further polymerization of the oligomer H-IM1-1·$(H_2O)_4$, the oligomer H-IM1-1·$(H_2O)_4$ is the main structure of

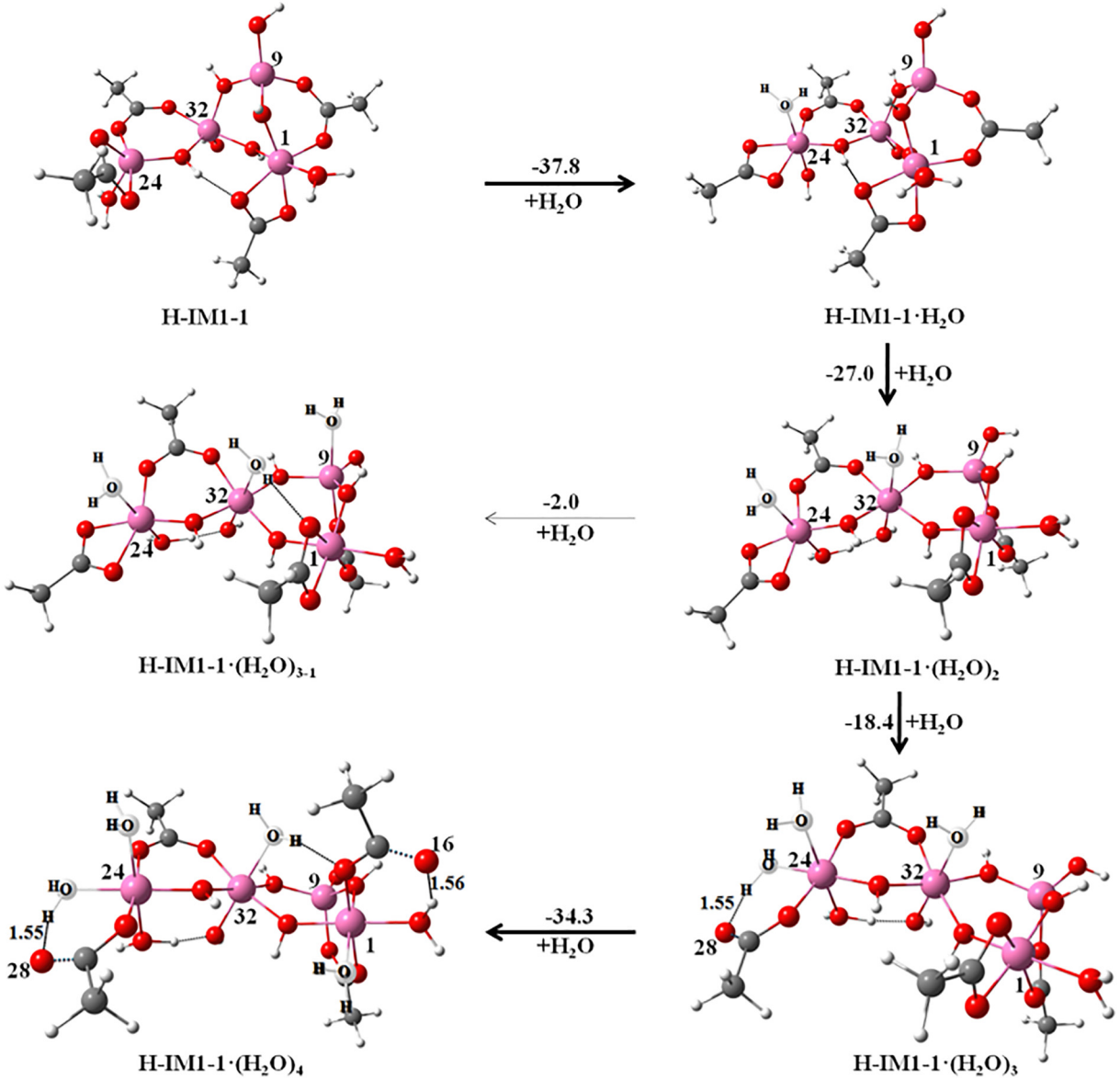


**Fig. 12.** Geometrical parameters and free energy differences of H-IM1-1·$(H_2O)_n$ (n = 1–4) in aqueous solution.

**Table 5**
Unscaled calculations for vibrational frequencies, IR intensities and band assignments of H-IM1-1·$(H_2O)_4$.

| Species | Assignment | Vibrational frequency (experimental frequency)/$cm^{-1}$ | IR intensity/km·$mol^{-1}$ |
|---|---|---|---|
| H-IM1-1·$(H_2O)_4$ | $CH_3$ (def.) | 1420 (1419) | 456 |
| | OCO (asym., str.) | 1581 (1594) | 940 |
| | OCO (sym., str.) | 1481 (1478) | 396 |
| | OH (Al-OH, def.) | 1030 (1031) | 337 |
| | OH (H-OH, str.) | 3401 (3421) | 1311 |
| | Al-O (AlO6, str.) | 641 (627) | 336 |
| | | 685 (697) | 404 |

the sol, and the proportion of octahedral to tetrahedral in this structure is approximately 3:1. However, the remaining two active hydroxyl groups on H-IM1-1·$(H_2O)_4$ could continue to polymerize to form linear polymers in the subsequent concentration process, which is beneficial to the spinnability of aluminium sols.

### *3.7. Structure formation of precursor sols when the ratio of $H^+$ to BAA2-2 is 2 in aqueous solution ($H^+$/BAA = 1, pH < 2.98)*

With increasing amounts of $H^+$, two hydroxyl groups of BAA2-2 are protonated by $H^+$ ions to form intermediate BAA2-2-2H, as shown in Fig. 13. BAA2-2-2H (b) is more stable than BAA2-2-2H (a) by 2.3 kJ/mol. This small energy difference indicates that both BAA2-2-2H (b) and BAA2-2-2H (a) exist with comparable ratios. However, BAA2-2-2H (a) is more stable than BAA2-2-2H (c) by 60.6 kJ/mol, indicating that almost no BAA2-2-2H (c) exists and that $H^+$ ions are more likely to protonate the hydroxyl groups of two different Al atoms of BAA2-2 to form the intermediate BAA2-2-2H.

#### *3.7.1. Coordination of water to BAA2-2-2H*

In this study, the coordination of BAA2-2-2H with different amounts of $H_2O$ was also investigated. All the species of BAA2-2-2H·$(H_2O)_n$ (n = 1–4) in aqueous solution were fully optimized; the geometrical parameters and free energy differences of BAA2-2-2H·$(H_2O)_n$ (n = 1–4) in aqueous solution are depicted in Fig. 14.

Fig. 14 indicates that BAA2-2-2H·$(H_2O)_2$ is more stable than the isomer BAA2-2-2H·$(H_2O)_{2\text{-}1}$ by 7.8 kJ/mol. Gradually adding one, two, three and four water molecules to BAA2-2-2H stabilize the Al complex by 47.8 kJ/mol, 39.9 kJ/mol, 46.7 kJ/mol and 20.6 kJ/mol, respectively. The BAA2-2-2H·$(H_2O)_4$, a new dimer of octahedral Al species, is the most stable hydrate. It is only when the fourth water molecule is added to BAA2-2-2H that the O16 atom in BAA2-2-2H·$(H_2O)_4$ is disconnected from the Al1 atom to form a hydrogen bond with a water molecule.

#### *3.7.2. Hydrolysis of the BAA2-2-2H*

Fig. 13 shows that the bond lengths between the Al1 and O3 in both BAA2-2-2H (b) and BAA2-2-2H (a) are shortened to 1.93 Å, as described in the hydrolysis of BAA2-2 and BAA2-2-H, which are hard to hydrolyse. However, we can also add two water molecules to the central Al1 atoms of BAA2-2-2H to study the hydrolysis kinetics of BAA2-2-2H. The optimized geometrical parameters and the PES profile of this channel are shown in Fig. 15. From Fig. 15 it can be seen that the hydrolysis kinetics of BAA2-2-2H are the same as those of BAA2-2-H. The barrier of this process is 109.1 kJ/mol. The 2H-2$H_2O$-IM2 molecule is more stable than 2H-2$H_2O$-IM3 + $CH_3COOH$ in free energy, which implies that the hydrolysed $CH_3COOH$ surrounds the BAA2-2-2H oligomers by hydrogen bonds until the hydrolysed $CH_3COOH$ is expelled by water molecules, such as how BAA2-2-H, BAA2-2-2H may be hydrolysed by adding two water molecules.

#### *3.7.3. Oligomerization of the BAA2-2-2H*

The polymerization of BAA2-2-2H with itself before forming hydrates with water molecules is also studied in this work, as shown in

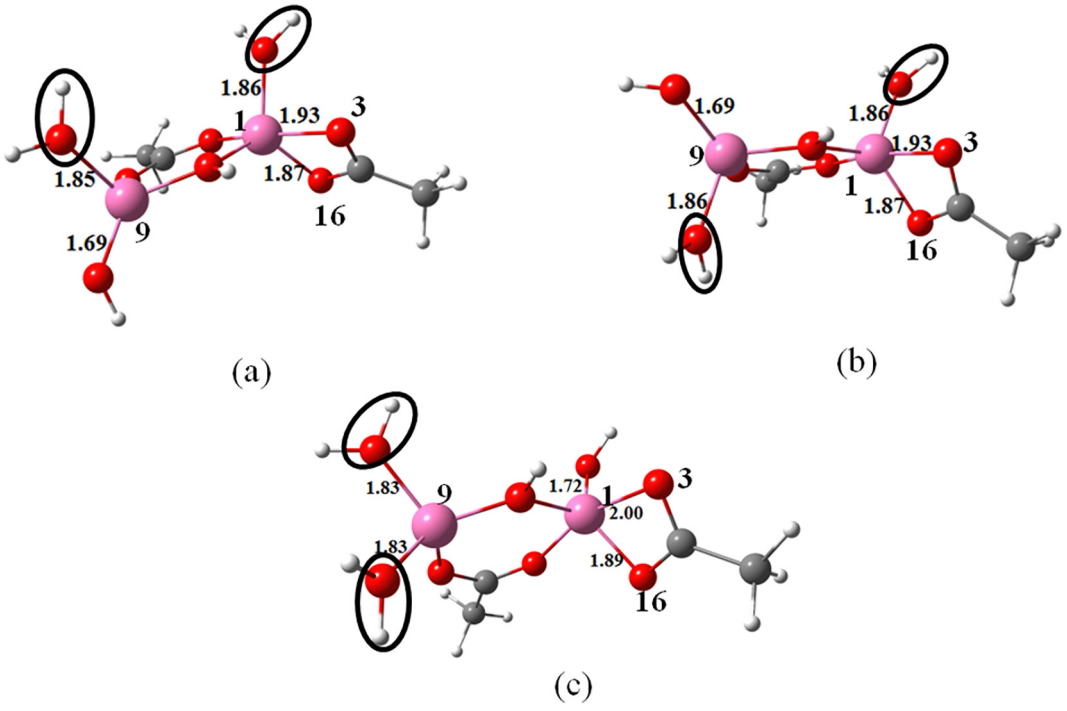


**Fig. 13.** Optimized geometries and selected bond distances of BAA2-2-2H in aqueous solution.

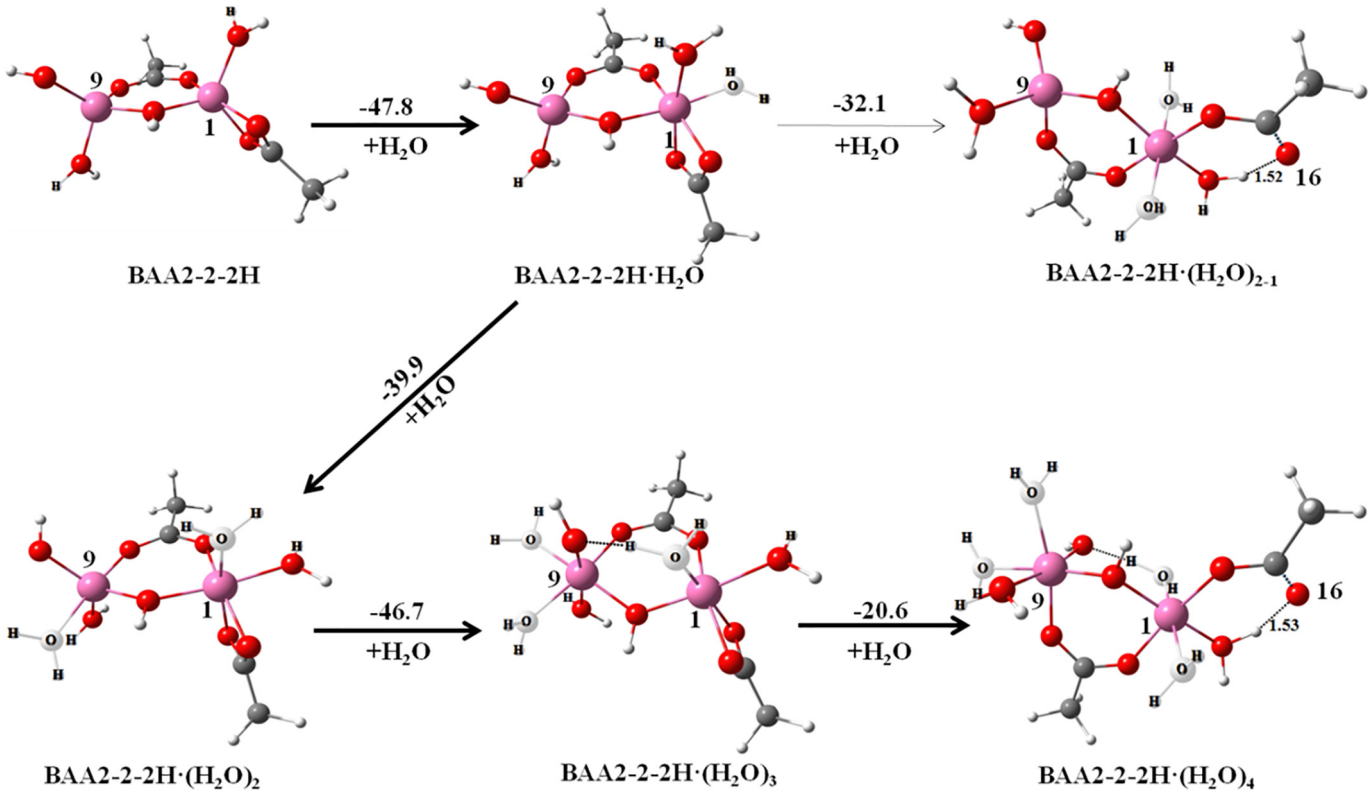


**Fig. 14.** Geometrical parameters and free energy differences of BAA2-2-2H·$(H_2O)_n$ (n = 1–4) in aqueous solution.

Fig. 16. Two BAA2-2-2H molecules are connected by the bridging O43 atom to form 2H-IM1, increasing the free energy by 21.5 kJ/mol. Then, the H44 diverts from O43 to O17 via transition-state 2H-TS1, leading to the formation of 2H-IM2. The transition-state energy barrier is 27.1 kJ/mol. Subsequently, a water molecule leaves the Al9 atom, and the product 2H-IM3 is obtained. Fig. 16 shows 2H-IM2 is the most stable species in this process.

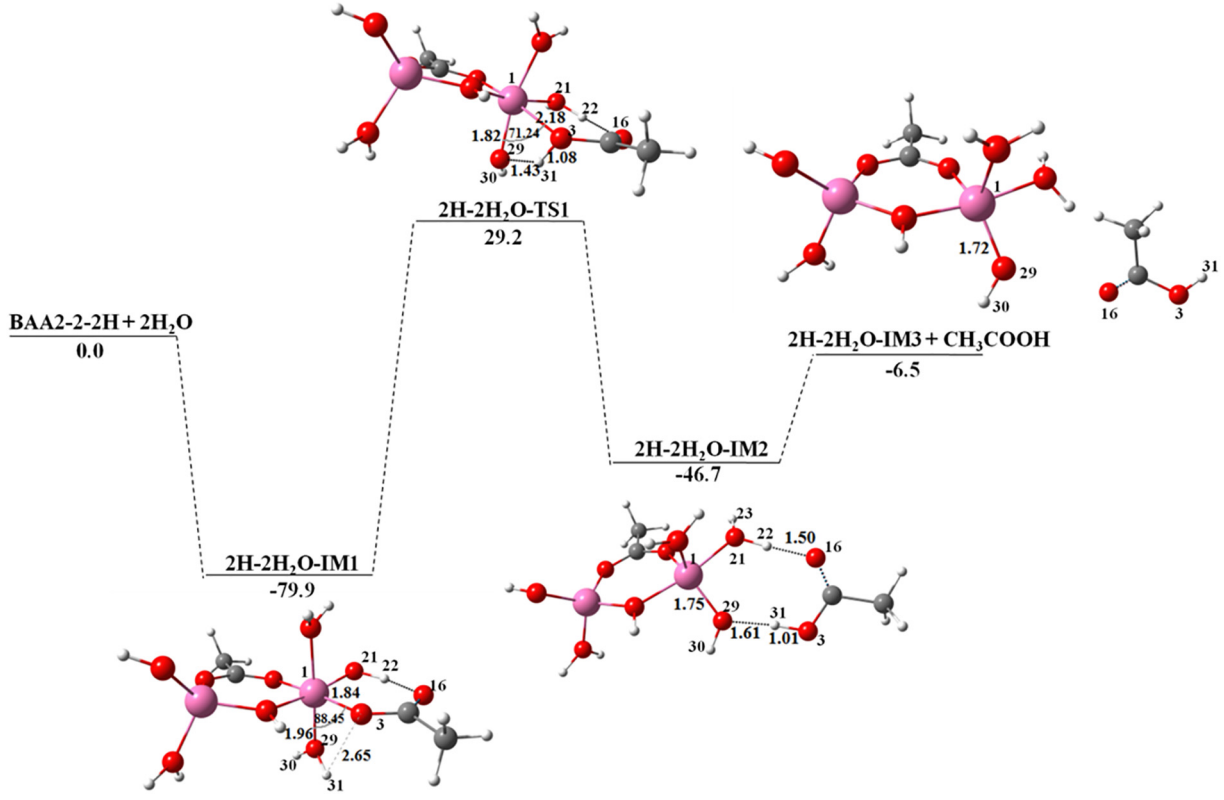


**Fig. 15.** Optimized geometrical parameters and the PES profile involved in the hydrolysis of BAA2-2-2H in aqueous solution.

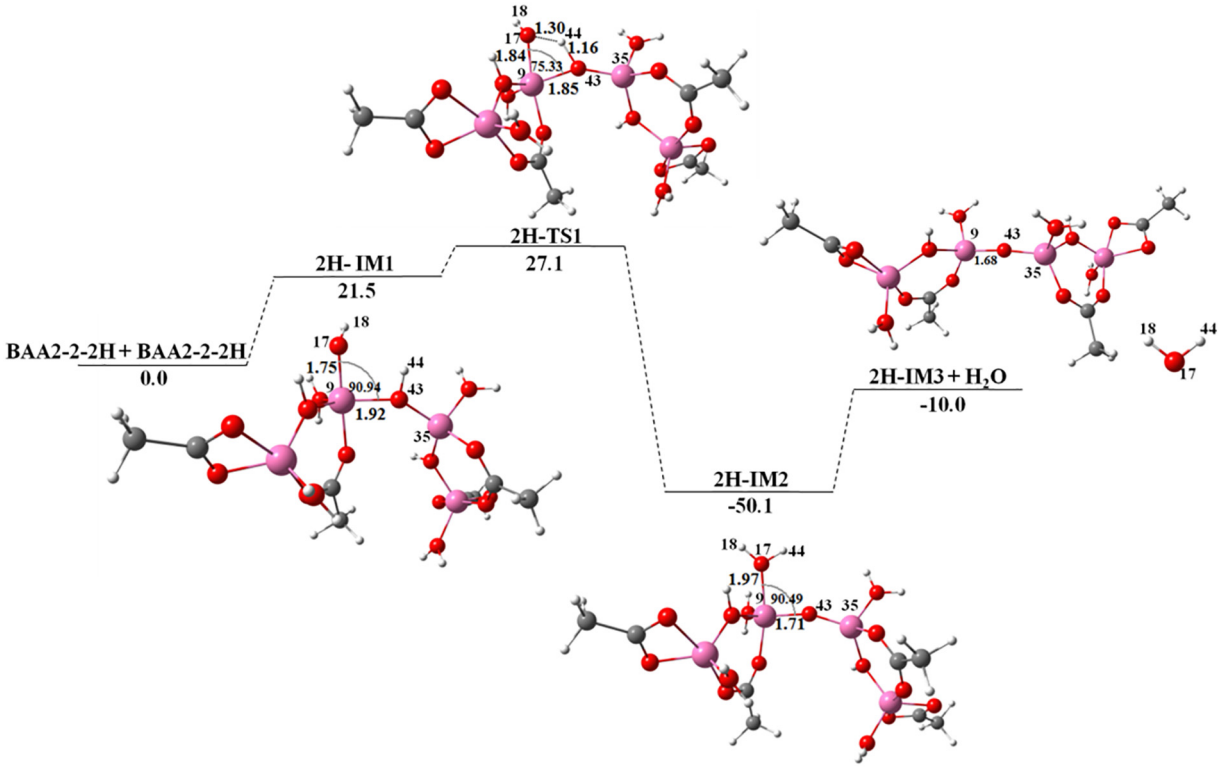


**Fig. 16.** Optimized geometrical parameters and the PES profile involved in the polymerization of BAA2-2-2H in aqueous solution.

As mentioned above, the addition of two $H^+$ ions changes the electronic properties of the Al9 and Al1 atoms, which significantly improves the coordination ability of water to the Al9 and Al1 ions. Compared with the hydrolysis and polymerization of BAA2-2-2H, it is easier to coordinate with water molecules one by one to form the hydrate BAA2-2-2H·$(H_2O)_4$. Since the coordination of water molecules with $Al^{3+}$ prevent further polymerization of the hydrate, the hydrate BAA2-2-2H·$(H_2O)_4$ is the main component of the sol when the ratio of $H^+$/BAA2-2 is 2 (the molar ratio of $H^+$/BAA is 1). The assignment of frequencies in the IR spectra of BAA2-2-2H·$(H_2O)_4$ are listed in Table 6. Due to the presence of high concentration of $NO_3^-$, the intensity of its stretching vibration is so strong that the deformation modes of the bands at 1422 $cm^{-1}$ and 1031 $cm^{-1}$ corresponding to $CH_3$ and O—H (Al—OH) almost disappeared in the experimental spectra. In addition, the hydroxyl peak (the band at 3446 $cm^{-1}$) in experiment is different from the hydroxyl peak (the band at 3864 $cm^{-1}$) calculated by DFT, which might due to the formation of hydrogen bonds between the water molecules on Al atom and the free water molecules before the FT-IR spectroscopic test. From Table 6, the IR intensity of O—H (Al—OH) is relatively weaker than that of H-IM1-1·$(H_2O)_4$, while that of Al—O (AlO6) is relatively stronger. These results provided by DFT calculation are in agreement with the FT-IR experimental results.

However, there are minor differences between the $^{27}Al$ NMR and above calculation results. From the $^{27}Al$ NMR spectra, the dimers began to appear when the molar ratio of $HNO_3$/BAA is <0.5 (Fig. 2, curve Sol 2), which may result because BAA2-2 tends to agglomerate and cannot be completely dissolved in aqueous solution instantaneously in the experiment, and two hydroxyl groups of the dissolved BAA2-2 are protonated by two $H^+$ ions to form the dimer of the octahedral Al species. Therefore, two suggestions could be put forward to improve the uniformity and spinnability of the precursor sols during the preparation of ceramic fibers: (1) preventing the BAA2-2 from agglomerating and accelerating the dissolution of BAA2-2; (2) finding other proton donors that can release $H^+$ ions according to the needs of BAA2-2.

## 4. Conclusions

In this work, colourless and transparent aluminium sols were prepared by the sol-gel method using BAA and $HNO_3$ as raw materials. FT-IR and $^{27}Al$ NMR spectroscopy were used to characterize the structure of the BAA and investigate the components of the aluminium precursor sols prepared with different molar ratios of $HNO_3$/BAA. The FT-IR measurements showed that BAA containing acetate ions act as bridging ligand; BAA might exist in dimeric form. $^{27}Al$ NMR showed that the relative contents of AlO6 including $Al^{3+}$ oligomers and dimers or monomers increased with the molar ratio of $HNO_3$/BAA from 0 to 0.75, as supported by the FTIR results; the relative content of $Al^{3+}$ oligomers (resonance at ~5 ppm) reached the maximum when the molar ratio of $HNO_3$/BAA was 0.5.

**Table 6**
Unscaled calculations for vibrational frequencies, IR intensities and band assignments of BAA2-2-2H·$(H_2O)_4$.

| Species | Assignment | Vibrational frequency (experimental frequency)/$cm^{-1}$ | IR intensity/km·$mol^{-1}$ |
|---|---|---|---|
| BAA2-2-2H·$(H_2O)_4$ | $CH_3$ (def.) | 1420 (—) | 412 |
| | OCO (asym., str.) | 1586 (1593) | 1051 |
| | OCO (sym., str.) | 1487 (1478) | 370 |
| | OH (Al-OH, def.) | 1034 (—) | 303 |
| | OH (H-OH, str.) | 3864 (3408) | 278 |
| | Al-O (AlO6, str.) | 691 (695) | 421 |

Combined with the analysis results of FT-IR and $^{27}Al$ NMR on BAA structure, DFT calculation was applied to study the hydrolysis and oligomerization mechanisms of BAA under neutral and acidic conditions. The DFT calculations found that the dimer BAA2-2 consisting of tetrahedral Al species was more stable than other dimeric isomers. In neutral aqueous solution, the hydrolysis of BAA2-2 was very difficult; the oligomers prepared by BAA2-2 could further react with themselves or BAA2-2 molecules to form different polymers with dendritic or other three-dimensional structures. In acidic aqueous solution, the hydrolysis of BAA2-2-H was possible, which agreed with the FT-IR results. The formation of oligomer H-IM1-1·$(H_2O)_4$ prepared by BAA2-2-H was more thermodynamically favourable than that of BAA2-2-H·$(H_2O)_2$. This oligomer comprised three octahedral and one tetrahedral Al species, and could continue to polymerize to form linear polymers in the subsequent concentration process, which was beneficial to the spinnability of the precursor sols during the preparation of ceramic fibers. The oligomers prepared from BAA2-2-2H ($H^+$/BAA, 1) were mostly determined to be a dimer of octahedral Al species due to the coordination of BAA2-2-2H with five water molecules. The addition of $H^+$ changed the electronic properties of Al(III) and significantly promoted the coordination ability of water and $Al^{3+}$, leading to an increase in the octahedral Al species and a great change in the structure of aluminium sols, which will have a significant impact on the structure and properties of the final materials. The vibrational frequencies and structure (tetrahedral or octahedral Al species) of BAA2-2 and its oligomers provided by DFT calculation were agreed with the experimental measurements. DFT calculations provided a necessary theoretical guidance for further improving the performance of aluminium precursor sols and meeting the needs of the final materials, and constituted a basis for further investigation on the mechanisms of the structural transformation from sols to gels.

## Declaration of Competing Interest

There are no conflicts to declare.

## Acknowledgements

The authors gratefully acknowledge the financial support from the “Chang Jiang Scholars Program” of the Ministry of Education of China (Grant no. T2011119).

## References

[1] H.G. Sowman, Aluminum borate and aluminum borosilicate articles, U.S. Patent 3,795,524, 1974.
[2] X. Song, Y. Cao, Q. Liu, J. Wang, S. Yao, W. Liu, Y. Ma, Q. Cai, Thermally stable boron-containing mullite fibers derived from a monophasic mullite sol, Ceram. Int. 45 (2019) 1171–1178, https://doi.org/10.1016/j.ceramint.2018.09.301.
[3] A.R. Bunsell, M.-H. Berger, Fine diameter ceramic fibres, J. Eur. Ceram. Soc. 20 (2000) 2249–2260, https://doi.org/10.1016/S0955-2219(00)00090-X.
[4] B. Clauss, D. Schawaller, Modern aspects of ceramic fiber development, Adv. Sci. Techno. 50 (2006) 1–8, https://doi.org/10.4028/www.scientific.net/AST.50.1.
[5] Y.H. Chiou, M.T. Tsai, H.C. Shih, The preparation of alumina fibre by sol-gel processing, J. Mater. Sci. 29 (1994) 2378–2388, https://doi.org/10.1007/BF00363430.
[6] J. Chandradass, M. Balasubramanian, Sol-gel processing of alumina fibres, J. Mater. Process Tech. 173 (2006) 275–280, https://doi.org/10.1016/j.jmatprotec.2005.11.030.
[7] X. Chen, L. Gu, Sol-gel dry spinning of mullite fibers from AN/TEOS/AIP system, Mater. Res. Bull. 44 (2009) 865–873, https://doi.org/10.1016/j.materresbull.2008.09.011.
[8] K.C. Song, Preparation of mullite fibers from aluminum isopropoxide–aluminum nitrate–tetraethylorthosilicate solutions by sol-gel method, Mater. Lett. 35 (1998) 290–296, https://doi.org/10.1016/S0167-577X(97)00268-1.
[9] H. Zhang, Y. Hang, Y. Qi, J. Yang, B. Wang, Synthesis and characterization of sol-gel derived continuous spinning alumina based fibers with silica nano-powders, J. Eur. Ceram. Soc. 34 (2014) 465–473, https://doi.org/10.1016/j.jeurceramsoc.2013.08.015.
[10] Y. Zhang, Y. Ding, J. Gao, J. Yang, Mullite fibres prepared by sol-gel method using polyvinyl butyral, J. Eur. Ceram. Soc. 29 (2009) 1101–1107, https://doi.org/10.1016/j.jeurceramsoc.2008.08.008.
[11] L.S. Cividanes, T.M.B. Campos, L.A. Rodrigues, D.D. Brunelli, G.P. Thim, Review of mullite synthesis routes by sol-gel method, J. Sol-Gel Sci. Technol. 55 (2010) 111–125, https://doi.org/10.1007/s10971-010-2222-9.
[12] A.E. Danks, S.R. Hallb, Z. Schnepp, The evolution of ‘sol–gel’ chemistry as a technique for materials synthesis, Mater. Horiz. 3 (2016) 91–112, https://doi.org/10.1039/c5mh00260e.
[13] S. Sakka, K. Kamiya, The sol-gel transition in the hydrolysis of metal alkoxides in relation to the formation of glass fibers and films, J. Non-Cryst. Solids 48 (1982) 31–46, https://doi.org/10.1016/0022-3093(82)90244-7.
[14] X. Chen, L. Gu, The sol-gel transition of mullite spinning solution in relation to the formation of ceramic fibers, J. Sol-Gel Sci. Technol. 46 (2008) 23–32, https://doi.org/10.1007/s10971-007-1666-z.
[15] H. Tan, Y. Ding, J. Yang, Mullite fibers prepared from an inorganic sol-gel precursor, J. Sol-Gel Sci. Technol. 53 (2009) 378–383, https://doi.org/10.1007/s10971-009-2106-z.
[16] R. Jószai, M. Purgel, I. Pápai, H. Wakita, I. Tóth, Multinuclear NMR and DFT studies of the structure and fluxionality for $M^{III}$ ethylenediamine tetraacetate complexes (M(EDTA)$^-$, M = Al, Ga and In) in solution, J. Mol. Liq. 131-132 (2007) 72–80, https://doi.org/10.1016/j.molliq.2006.08.030.
[17] S. Munsif, K. Ayub, Diffusion of alkali metal atoms (Li, Na, K) on aluminium nitride and boron nitride nanocages; a density functional theory study, J. Mol. Liq. 259 (2018) 249–259, https://doi.org/10.1016/j.molliq.2018.03.009.
[18] X. Cheng, D. Chen, Y. Liu, Mechanisms of silicon alkoxide hydrolysis-oligomerization reactions: a DFT investigation, Chemphyschem 13 (2012) 2392–2404, https://doi.org/10.1002/cphc.201200115.
[19] C.E. White, J.L. Provis, G.J. Kearley, D.P. Riley, van J.S.J. Deventer, Density functional modelling of silicate and aluminosilicate dimerisation solution chemistry, Dalton Trans. 40 (2011) 1348–1355, https://doi.org/10.1039/C0DT01042A.
[20] W. Liu, Y. Li, Y. Ma, J. Wang, T. Luo, S. Xu, Effect of sintering temperature on microstructure and properties of boron aluminum silicate fibers, J. Chin. Ceram. Soc. 45 (2017) 847–854, https://doi.org/10.14062/j.issn.0454-5648.2017.06.15.
[21] M.J. Frisch, G.W. Trucks, H.B. Schlegel, G.E. Scuseria, M.A. Robb, J.R. Cheeseman, V.G. Zakrzewski, J.A. Montgomery, R.E. Stratmann, J.C. Burant, S. Dapprich, J.M. Millam, A.D. Daniels, K.N. Kudin, M.C. Strain, O. Farkas, J. Tomasi, V. Barone, M. Cossi, R. Cammi, B. Mennucci, C. Pomelli, C. Adamo, S. Clifford, J. Ochterski, G.A. Petersson, P.Y. Ayala, Q. Cui, K. Morokuma, D.K. Malick, A.D. Rabuck, K. Raghavachari, J.B. Foresman, J. Cioslowski, J.V. Oritz, B. Stefanov, G. Liu, A. Liashenko, P. Piskorz, I. Komaromi, R. Gomperts, R.L. Martin, D.J. Fox, T. Keith, M.A. Al-Laham, C.Y. Peng, A. Nanayakkara, C. Gonzalez, M. Challacombe, P.M.W. Gill, B.G. Johnson, W. Chen, M.W. Wong, J.L. Andres, M. Head-Gordon, E.S. Replogle, J.A. Pople, Gaussian 03, Gaussian, Inc., Wallingford, CT, 2004.
[22] V. Barone, M. Cossi, Quantum calculation of molecular energies and energy gradients in solution by a conductor solvent model, J. Phys. Chem. A 102 (1998) 1995–2001, https://doi.org/10.1021/jp9716997.
[23] M. Cossi, N. Rega, G. Scalmani, V. Barone, Energies, structures, and electronic properties of molecules in solution with the C-PCM solvation model, J. Comput. Chem. 24 (2003) 669–681, https://doi.org/10.1002/jcc.10189.
[24] M. Nora, M. Fatiha, N. Leila, H. Sakina, K. DjamelEddine, Density functional study of inclusion complex of albendazole/cucurbit [7] uril: structure, electronic properties, NBO, GIAO and TD-DFT analysis, J. Mol. Liq. 211 (2015) 40–47, https://doi.org/10.1016/j.molliq.2015.06.054.
[25] Y. Takano, K.N. Houk, Benchmarking the conductor-like polarizable continuum model (CPCM) for aqueous solvation free energies of neutral and ionic organic molecules, J. Chem. Theory Comput. 1 (2005) 70–77, https://doi.org/10.1021/ct049977a.
[26] X. Cheng, Y. Liu, D. Chen, Mechanisms of hydrolysis-oligomerization of aluminum alkoxide Al$(OC_3H_7)_3$, J. Phys. Chem. A 115 (2011) 4719–4728, https://doi.org/10.1021/jp110848e.
[27] K. Fukui, The path of chemical reactions - the IRC approach, Acc. Chem. Res. 14 (1981) 363–368, https://doi.org/10.1021/ar00072a001.
[28] C. Gonzalez, H.B. Schlegel, Reaction path following in mass-weighted internal coordinates, J. Phys. Chem. 94 (1990) 5523–5527, https://doi.org/10.1021/j100377a021.
[29] P. Persson, M. Karlsson, L.O. Öhman, Coordination of acetate to Al(III) in aqueous solution and at the water-aluminum hydroxide interface: a potentiometric and attenuated total reflectance FTIR study, Geochim. Cosmochim. Acta 62 (1998) 3657–3668, https://doi.org/10.1016/S0016-7037(98)00260-9.
[30] S. Dubey, M. Agarwal, A.B. Gupta, Experimental investigation of Al-F species formation and transformation during coagulation for fluoride removal using alum and PACl, J. Mol. Liq. 266 (2018) 349–360, https://doi.org/10.1016/j.molliq.2018.06.080.
[31] S. Sanati, Z. Rezvani, Co-intercalation of Acid Red-27/sodium dodecyl sulfate in a Ce-containing Ni-Al-layered double hydroxide matrix and characterization of its luminescent properties, J. Mol. Liq. 249 (2018) 318–325, https://doi.org/10.1016/j.molliq.2017.10.145.
[32] H.S. Song, J. Zhang, J. Lin, S.J. Liu, J.J. Luo, Y. Huang, E.M. Elssfah, A. Elsanousi, X.X. Ding, J.M. Gao, C. Tang, Coating aluminum borate ($Al_{18}B_4O_{33}$) nanowire webs with BN, J. Phys. Chem. C 111 (2007) 1136–1139, https://doi.org/10.1021/jp067393u.
[33] M. Potangale, A. Das, S. Kapoor, S. Tiwari, Effect of anion and alkyl chain length on the structure and interactions of N-alkyl pyridinium ionic liquids, J. Mol. Liq. 240 (2017) 694–707, https://doi.org/10.1016/j.molliq.2017.05.036.
[34] S. Hou, S. Tong, Y. Zhang, F. Tan, Y. Guo, M. Ge, Heterogeneous uptake of gas-phase acetic acid on the surface of α-$Al_2O_3$ particles: temperature effects, Chem. Asian J. 11 (2016) 2749–2755, https://doi.org/10.1002/asia.201600402.
[35] R. Venkatesh, S.R. Ramanan, Effect of organic additives on the properties of sol-gel spun alumina fibres, J. Eur. Ceram. Soc. 20 (2000) 2543–2549, https://doi.org/10.1016/S0955-2219(00)00135-7.

[36] M.J. Tafreshi, Z.M. Khanghah, Infrared spectroscopy studies on sol-gel prepared alumina powders, Mater. Sci. 21 (2015) 28–31, https://doi.org/10.5755/j01.ms.21.1.4872.
[37] P.P. Nampi, P. Moothetty, F.J. Berry, M. Mortimerc, K.G. Warriera, Aluminosilicates with varying alumina-silica ratios: synthesis via a hybrid sol–gel route and structural characterisation, Dalton Trans. 39 (2010) 5101–5107, https://doi.org/10.1039/C001219J.
[38] F. Dumeignil, M. Rigole, M. Guelton, J. Grimblot, Characterization of boria-alumina mixed oxides prepared by a sol-gel method. 1. NMR characterization of the xerogels, Chem. Mater. 17 (2005) 2361–2368, https://doi.org/10.1021/cm048080j.
[39] M. Ibrahim, E. Koglin, Vibrational spectroscopic study of acetate group, Acta Chim. Slov. 51 (2004) 453–460.
[40] V.A. Minaeva, B.F. Minaeva, G.V. Baryshnikov, O.M. Romeyko, M. Pittelkow, The FTIR spectra of substituted tetraoxa [8] circulenes and their assignments based on DFT calculations, Vib. Spectrosc. 65 (2013) 147–158, https://doi.org/10.1016/j.vibspec.2013.01.001.